Table 1. Estimates of ion density n, temperature T, and pressure P for the cusp (C) and equatorial (E) regions shown in Figs. 3 and 4.

Date (2011)		H^+			Na group		
		n (cm^{-3})	T (MK)	P (nPa)	n (cm^{-3})	T (MK)	P (nPa)
13 April	C	12	1.3	0.22	*	*	*
14 April	C	20	0.79	0.21	*	*	*
16 April	C	40	0.79	0.44	0.5	1	0.008
13 April	E	1.5	5.1	0.11	†	†	†
15 April	E	1.6	3.6	0.079	0.2	1–3	0.003–0.008
21 April	E	0.28	7.8	0.030	0.3	3	0.01

*Too few counts. †Substantial bulk velocity violates assumptions for data inversion.

plasma is expected to be transported preferentially through the magnetically dominated lobe regions and concentrated in the plasma sheet at low latitudes. The plasma sheet is threaded by closed planetary magnetic fields such that its northward component combined with the dawn-to-dusk electric field imposed by the global solar wind interaction result in a sunward magnetic stress. This stress is balanced by a tailward-directed gradient in the plasma pressure (i.e., plasma density and temperature decrease with increasing downtail distance).

The heavy-ion observations provide important constraints for Mercury's neutral exosphere and its temporal variability and spatial distribution. Single-particle calculations indicate that He^+ and O^+ ion fluxes could be comparable if the near-surface density of neutral oxygen does not exceed 200 atoms cm^{-3}, as predicted by exosphere models (*14*, *16*). From the observed spatial distributions, the energy of the observed ions, and comparisons with observations of the neutral exosphere, we conclude that the planetary ions discussed here are being created by the ionization of exospheric neutral species. Moreover, MESSENGER observations reveal that Mercury's cusps act as natural collection points and conduits for solar wind and planetary ions, such as the O group, Na group, and other ions, that are likely to contribute to the neutral exosphere as they precipitate onto the planetary surface. There are orbit-to-orbit differences in observations, which reflect the magnetospheric response to a highly variable solar wind (*17*) and which are anticipated from the temporal variability of Earth-based observations of the Na exosphere (*6*). Given the high heavy-ion thermal pressures relative to proton pressures at Mercury reported here, the role of heavy ions must be included to properly understand the dynamics of Mercury's magnetosphere.

References and Notes

1. B. J. Anderson *et al.*, *Science* **333**, 1859 (2011).
2. J. A. Slavin *et al.*, *Science* **321**, 85 (2008).
3. K. Kabin, T. I. Gombosi, D. L. DeZeeuw, K. G. Powell, *Icarus* **143**, 397 (2000).
4. L. A. Frank, *J. Geophys. Res.* **76**, 5202 (1971).
5. G. Haerendel, G. Paschmann, N. Sckopke, H. Rosenbauer, P. C. Hedgecock, *J. Geophys. Res.* **83**, (A7), 3195 (1978).
6. R. Killen *et al.*, *Space Sci. Rev.* **132**, 433 (2007).
7. A. Lukyanov, S. Barabash, M. Holmström, *Adv. Space Res.* **33**, 1890 (2004).
8. J. A. Slavin *et al.*, *Science* **329**, 665 (2010).
9. D. C. Delcourt *et al.*, *Planet. Space Sci.* **55**, 1502 (2007).
10. G. B. Andrews *et al.*, *Space Sci. Rev.* **131**, 523 (2007).
11. T. H. Zurbuchen *et al.*, *Science* **321**, 90 (2008).
12. E. Möbius *et al.*, *Astron. Astrophys.* **426**, 897 (2004).
13. R. E. Hartle, S. A. Curtis, G. E. Thomas, *J. Geophys. Res.* **80**, 3689 (1975).
14. M. Sarantos, P. H. Reiff, T. W. Hill, R. M. Killen, A. L. Urquhart, *Planet. Space Sci.* **49**, 1629 (2001).
15. J. M. Raines *et al.*, *Planet. Space Sci.* (2011); 10.1016/j.pss.2011.02.004.
16. P. Wurz *et al.*, *Planet. Space Sci.* **58**, 1599 (2010).
17. D. N. Baker *et al.*, *Planet. Space Sci.* (2011); 10.1016/j.pss.2011.01.018.

Acknowledgments: The MESSENGER project is supported by the NASA Discovery Program under contracts NAS5-97271 to The Johns Hopkins University Applied Physics Laboratory and NASW-00002 to the Carnegie Institution of Washington.

18 July 2011; accepted 6 September 2011
10.1126/science.1211302

MESSENGER Observations of Transient Bursts of Energetic Electrons in Mercury's Magnetosphere

George C. Ho,[1]* Stamatios M. Krimigis,[1,2] Robert E. Gold,[1] Daniel N. Baker,[3] James A. Slavin,[4,5] Brian J. Anderson,[1] Haje Korth,[1] Richard D. Starr,[6] David J. Lawrence,[1] Ralph L. McNutt Jr.,[1] Sean C. Solomon[7]

The MESSENGER spacecraft began detecting energetic electrons with energies greater than 30 kilo–electron volts (keV) shortly after its insertion into orbit about Mercury. In contrast, no energetic protons were observed. The energetic electrons arrive as bursts lasting from seconds to hours and are most intense close to the planet, distributed in latitude from the equator to the north pole, and present at most local times. Energies can exceed 200 keV but often exhibit cutoffs near 100 keV. Angular distributions of the electrons about the magnetic field suggest that they do not execute complete drift paths around the planet. This set of characteristics demonstrates that Mercury's weak magnetic field does not support Van Allen–type radiation belts, unlike all other planets in the solar system with internal magnetic fields.

The three flybys of Mercury by Mariner 10 in 1974 and 1975 established that the innermost planet in the solar system hosts a dominantly dipolar magnetic field (*1*). No radiation belt similar to Earth's Van Allen belts was detected, although bursts of energetic particles were identified from observations during the first flyby (*2*). These observations included four high-energy particle events, which were identified as consisting of electrons (with energies >300 keV) and protons (>550 keV). It was later pointed out (*3*) that the responses of the Mariner 10 detectors were consistent with pile-up of lower-energy (<170-keV) electrons, so energetic protons may not have been measured. The MESSENGER spacecraft, inserted into orbit about Mercury on 18 March 2011, carries detectors designed to provide measurements of the energetic particle population. In particular, the Energetic Particle Spectrometer (EPS), one of two sensors on the Energetic Particle and Plasma Spectrometer instrument (*4*), measures electrons from ~25 keV to 1 MeV and ions from ~25 keV to ~2.75 MeV (*5*).

Shortly after MESSENGER initiated scientific observations from orbit, EPS began recording recurring bursts of energetic electrons (Fig. 1). The first burst occurred on 27 March, and subsequent bursts were seen during each ~12-hour orbit on following days. From 26 March to 4 June, EPS detected more than 90 electron events. During these bursts, the measured electron intensity at energies less than 100 keV increased by one

[1]The Johns Hopkins University Applied Physics Laboratory, Laurel, MD 20723, USA. [2]Office of Space Research and Technology, Academy of Athens, Athens 11527, Greece. [3]Laboratory for Atmospheric and Space Physics, University of Colorado, Boulder, CO 80303, USA. [4]Heliophysics Science Division, NASA Goddard Space Flight Center, Greenbelt, MD 20771, USA. [5]Department of Atmospheric, Oceanic and Space Sciences, University of Michigan, Ann Arbor, MI 48109, USA. [6]Physics Department, The Catholic University of America, Washington, DC 20064, USA. [7]Department of Terrestrial Magnetism, Carnegie Institution of Washington, Washington, DC 20015, USA.

*To whom correspondence should be addressed. E-mail: george.ho@jhuapl.edu

to three orders of magnitude above background within a few seconds. For several events, the intensity increases extended to energies as great as 200 keV, as seen on 28 and 30 March (Fig. 1). The bursts typically lasted from a few seconds to several minutes and often came in groups spread over time intervals as long as several hours, as illustrated in Fig. 2A for an event on 29 March. The main group of electron bursts on that day occurred from ~0200 to 0225 Coordinated Universal Time (UTC) at local afternoon and mid-latitudes (Fig. 2C). A second, smaller group was detected at ~0230 UTC just after local midnight, and a much shorter-duration third group was seen at ~0237 UTC. These last two groups were seen near the magnetic equator, on the basis of analysis of magnetic field observations (*6*). Each of these individual electron bursts exhibited fine structure on time scales comparable to or shorter than the time resolution of EPS (3 s).

The angle between the observed particle velocity vector and the in situ magnetic field for most of these particles was ~45° to 135°, indicating that the electrons gyrate mostly perpendicular to the magnetic field line (Fig. 2B). The event-integrated electron-flux spectrum $j(E)$ is characterized by a power-law distribution ($dj/dE = kE^{-\gamma}$, where E is energy, k is a constant, and $\gamma \sim 3$) extending from the lowest-energy channel of EPS (~30 keV) up to >100 keV, as shown in Fig. 2D for the second group of events on 29 March. Other instruments on MESSENGER designed to detect x-rays, neutrons, and gamma-rays for remote sensing of planetary surface chemistry (*7*, *8*)

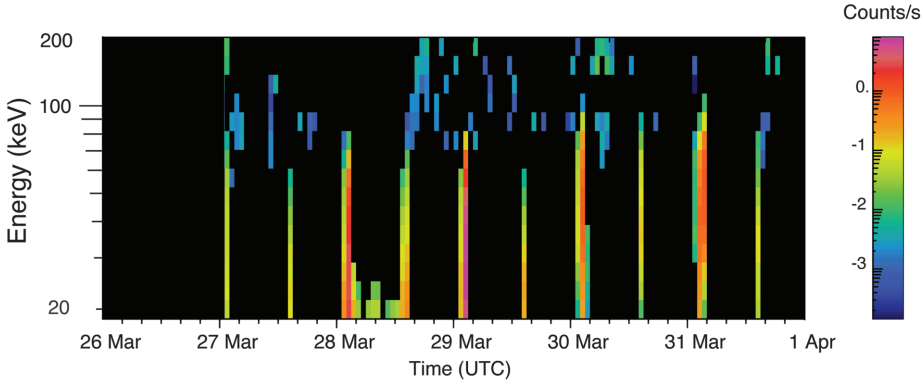

Fig. 1. Energy spectrogram for the electron events, corrected for cosmic-ray background, observed by EPS from 26 March to 1 April 2011. MESSENGER's orbital period at Mercury is ~12 hours, and the longer tic marks denote the beginning of the dates indicated.

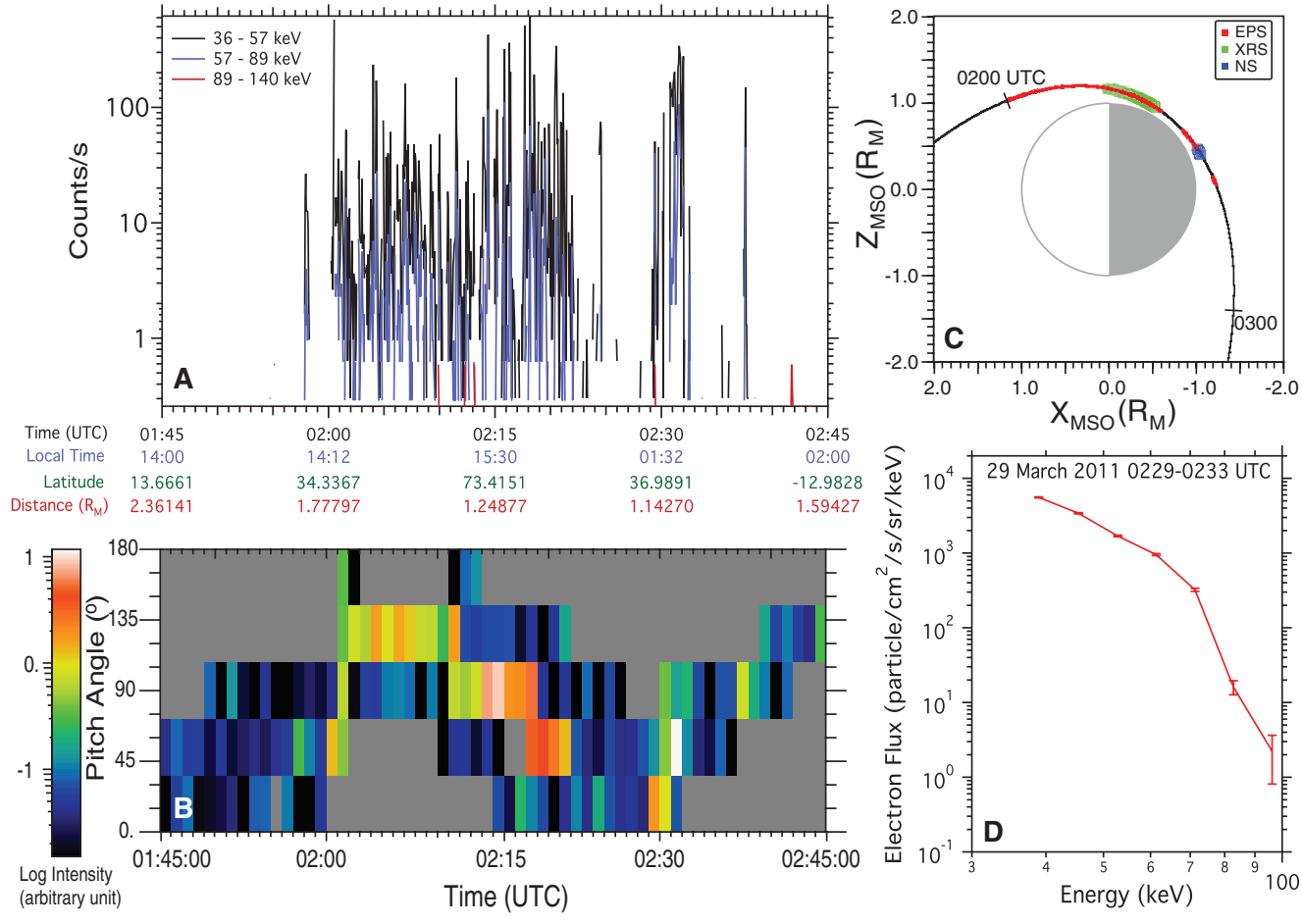

Fig. 2. Profiles of (**A**) intensity versus time, (**B**) pitch-angle distribution, (**C**) spacecraft location, and (**D**) energy spectrum for the electron bursts observed on 29 March 2011. Locations are shown in Mercury solar orbital (MSO) coordinates, for which *X* points sunward, *Z* northward, and *Y* duskward. Three groups of bursts were observed by EPS during the period from 0200 to 0237 UTC [red in (C)] as the spacecraft transited from the equatorial to the polar region of the planet. The same electron bursts were also detected on MESSENGER's XRS [green in (C)] and Neutron Spectrometer [(NS), blue in (C)]. The electron-flux spectrum is from a 4-min integration interval during the second group of electron events observed on 29 March 2011.

are also sensitive to electrons through energetic-electron–induced fluorescence and bremsstrahlung in their detectors, and observations with those instruments corroborated and enhanced the EPS measurements (Fig. 2C).

The energetic electron bursts have been seen over a broad range of northern (10° to 80°N) latitudes relative to Mercury's geographic equator. The most intense events were recorded at higher northern latitudes when the spacecraft was near periapsis. Those events recorded by EPS at southern latitudes, where the spacecraft is at much higher altitudes, have intensity levels that are typically an order of magnitude lower than those of the northern hemisphere events.

The coordinate system that best organizes particle data in a magnetosphere is the $|B|,L$ system (*9*), where $|B|$ is the magnetic field strength and L is the distance (in planetary radii) at which a dipole field line crosses the magnetic equator (*10*).

The distribution of energetic events in the $|B|,L$ system on Mercury's dayside and nightside is shown in Fig. 3. The most intense events on the nightside were seen close to the planet and near the magnetic equator (*11*). There were, however, some events at high latitudes but close to the planet, such as the one at $L = 1.6$. At high latitudes, the magnetic field lines are highly distorted from those for a dipolar field and are likely to be open, that is, linked to the solar wind rather than the opposite hemisphere of the planet. The large event at $L = 3.3$ was close to the nightside equator but could reflect a transient magnetospheric configuration.

The events on the dayside were mostly away from the equatorial plane and located at larger values of L. Given the compression of the magnetosphere on the dayside by solar-wind pressure, this distribution is unexpected. Only three relatively weak events were seen at the magnetic equator close to the planet. The events at higher latitudes and larger L values (>2) probably occurred on magnetic field lines that connected to the distended equatorial plasma sheet on the nightside.

The energetic particle data accumulated during MESSENGER's first Mercury year (88 Earth days) of observations show that the magnetosphere of Mercury is in a different class from those of Earth and the outer planets (*12*). At energies >30 keV, there appear to be no steady-state particle distributions in any particular location. Instead, intensities vary on time scales of ~3 s and perhaps less during events that persist intermittently for periods ranging from minutes to hours, close to the planet at high-to-intermediate northern latitudes but also at the equator, especially on the nightside. There is no evidence that the electron population undergoes full 360° drifts around the planet, although this inference is somewhat limited by MESSENGER's near-polar orbit. Hence, there are no electron radiation belts surrounding Mercury similar to the Van Allen belts at Earth. Moreover, no energetic ions with energy $E > 25$ keV above the detector intensity threshold have been identified thus far. Lower-energy (<10-keV) plasma ions are present throughout the magnetosphere (*13*), but they do not appear to be energized to the higher energies anticipated by most acceleration mechanisms, such as betatron or X- and O-type reconnection (*14*). One might have expected that protons would also be accelerated to similar energies, yet none have been observed so far. This situation is specific to Mercury's magnetosphere and is perhaps a result of the weakness of the planetary field and the consequently small magnetosphere dimensions.

The identity, location, and recurrent nature of these burstlike events suggest that there is an efficient acceleration mechanism operating within Mercury's magnetosphere on a regular basis that produces electrons with energies up to hundreds of kilo–electron volts, or ~10 times higher than could be imparted by the electric potential (~30 kV) applied to the system by solar-wind interaction (*15*), on time scales of seconds. Similar bursts of energetic electrons, but counterstreaming with protons, have been observed within Earth's magnetosphere (*16*, *17*). Simple scaling of phenomena from Earth's magnetosphere, although applicable for some processes (*15*), does not apply readily to energetic particle acceleration because Mercury has no trapped energetic particle population. Acceleration mechanisms have been proposed to explain the energetic particle observations made by Mariner 10 (*18*–*20*), but the limited observations by Mariner 10 did not strongly constrain any of the suggested mechanisms. MESSENGER's observations of energetic electrons in Mercury's magnetosphere provide a different example of rapid acceleration phenomena in a planetary magnetosphere with a length scale that is very much smaller than all others and may indicate a mechanism different from those established at other systems.

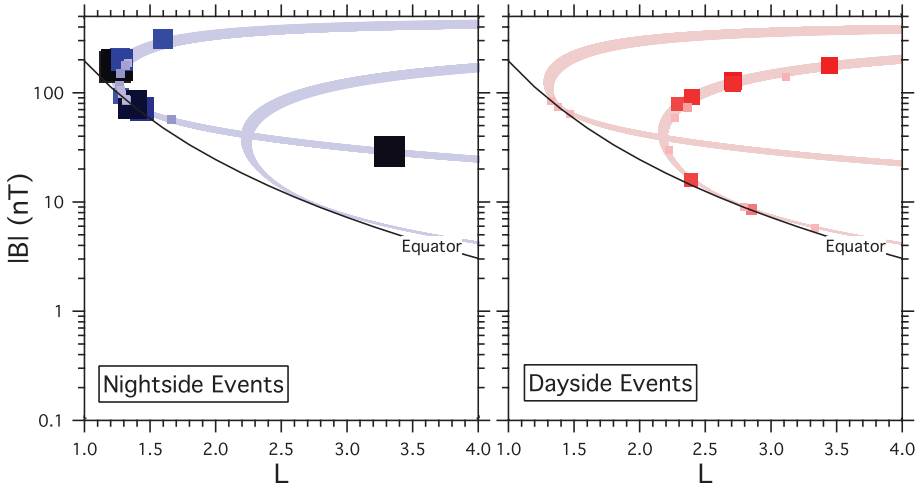

Fig. 3. Locations of the 92 electron events observed by EPS between 27 March and 3 June 2011 are plotted in $|B|,L$ coordinates (see text) for an offset-dipole representation of Mercury's magnetic field for both dayside (**right**) and nightside (**left**) events. The event intensity is represented by both the color and size of the marker, with darker and larger symbols indicating more intense events. The solid black line shows the magnetic equator at Mercury (*6*). The shaded areas denote regions of the space defined by this coordinate system that have been surveyed by MESSENGER.

References and Notes

1. N. F. Ness, K. W. Behannon, R. P. Lepping, Y. C. Whang, K. H. Schatten, *Science* **185**, 151 (1974).
2. J. A. Simpson, J. H. Eraker, J. E. Lamport, P. H. Walpole, *Science* **185**, 160 (1974).
3. T. P. Armstrong, S. M. Krimigis, L. J. Lanzerotti, *J. Geophys. Res.* **80**, 4015 (1975).
4. G. B. Andrews *et al.*, *Space Sci. Rev.* **131**, 523 (2007).
5. Before orbit insertion, MESSENGER completed three flybys of Mercury in 2008 and 2009. During these flybys, EPS detected no increases in particle intensity above instrumental background at any time during MESSENGER's near-equatorial magnetospheric passages (*15*, *21*). Fluorescent x-ray events seen by MESSENGER's X-Ray Spectrometer (XRS) during the flybys indicated the presence of suprathermal plasma (tens of kilo–electron volts) electrons inside Mercury's magnetosphere below the EPS energy-detection threshold (*21*).
6. B. J. Anderson *et al.*, *Science* **333**, 1859 (2011).
7. L. R. Nittler *et al.*, *Science* **333**, 1847 (2011).
8. P. N. Peplowski *et al.*, *Science* **333**, 1850 (2011).
9. C. E. McIlwain, *J. Geophys. Res.* **66**, 3681 (1961).
10. The $|B|,L$ system (*9*) for Mercury is well described by the offset dipole model (*6*), which gives $|B| = M\{3(Z_M/R)^2 + 1\}^{1/2}/R^3$ and $L = R/\{1 - (Z_M/R)^2\}$, where $R = \sqrt{X^2 + Y^2 + Z_M^2}$ is the radial distance from the center of the magnetic dipole in a Cartesian coordinate system (X,Y,Z) co-centered with the planet; the dipole moment M is 195 nT – R_M^3 (where R_M is Mercury's radius); the vertical component Z_M of the radius vector from the dipole is $Z - Z_0$, where Z is the component of the radius vector from the center of the planet normal to the planetary orbit; and the dipole offset Z_0 is 484 km northward. Because of the small size of the magnetosphere and the distortion of the magnetic field from that of a dipole, the L parameter represents the equatorial crossing point for only $L \lesssim 2$ but provides a useful indication of the approximate magnetic latitude of the field line threading the spacecraft even for $L > 2$.
11. The proximity of the largest events to Mercury's magnetic equator could account for the fact that EPS detected no increases in particle intensity above instrumental background during MESSENGER's three Mercury flybys in 2008 and 2009. All three flybys followed trajectories with closest approach on the nightside of the planet near the geographic equator, 484 km south of the magnetic equator.
12. B. H. Mauk, N. J. Fox, *J. Geophys. Res.* **115**, A12220 (2010).

13. T. H. Zurbuchen *et al.*, *Science* **333**, 1862 (2011).
14. M. Hoshino, S. Zenitani, K. Nagata, Y. Takagi, in *Energy Budget in the High Energy Universe*, K. Sato, J. Hisano, Eds. (World Scientific, Singapore, 2007), pp. 108–118.
15. J. A. Slavin *et al.*, *Science* **329**, 665 (2010); 10.1126/science.1188067.
16. S. M. Krimigis, E. T. Sarris, in *Dynamics of the Magnetosphere*, S. I. Akasofu, Ed. (D. Reidel, Dordrecht, Netherlands, 1979), pp. 599–630.
17. E. T. Sarris, S. M. Krimigis, T. Iijima, C. O. Bostrom, T. P. Armstrong, *Geophys. Res. Lett.* **3**, 437 (1976).
18. S. P. Christon, J. Feynman, J. A. Slavin, in *Magnetotail Physics*, A. T. Y. Lui, Ed. (Johns Hopkins Univ. Press, Baltimore, MD, 1987), pp. 393–400.
19. D. N. Baker, J. E. Borovsky, J. O. Burns, G. R. Gisler, M. Zeilik, *J. Geophys. Res.* **92**, 4707 (1987).
20. G. L. Siscoe, N. F. Ness, C. M. Yeates, *J. Geophys. Res.* **80**, 4359 (1975).
21. G. C. Ho *et al.*, *Planet. Space Sci.*, 31 January 2011 (10.1016/j.pss.2011.01.011).

Acknowledgments: We thank the MESSENGER team for the development, cruise, orbit insertion, and Mercury orbital operations of the MESSENGER spacecraft. G.C.H. thanks M. Johnson, L. Brown, and J. Vandegriff for graphics support. The NASA Discovery Program under contract NAS5-97271 to The Johns Hopkins University Applied Physics Laboratory and contract NASW-00002 to the Carnegie Institution of Washington supports the MESSENGER mission to Mercury. MESSENGER data are available from NASA's Planetary Data System archive.

13 July 2011; accepted 5 September 2011
10.1126/science.1211141

Evidence of Water Vapor in Excess of Saturation in the Atmosphere of Mars

L. Maltagliati,[1]* F. Montmessin,[1] A. Fedorova,[2] O. Korablev,[2] F. Forget,[3] J.-L. Bertaux[1]

The vertical distribution of water vapor is key to the study of Mars' hydrological cycle. To date, it has been explored mainly through global climate models because of a lack of direct measurements. However, these models assume the absence of supersaturation in the atmosphere of Mars. Here, we report observations made using the SPICAM (Spectroscopy for the Investigation of the Characteristics of the Atmosphere of Mars) instrument onboard Mars Express that provide evidence of the frequent presence of water vapor in excess of saturation, by an amount far surpassing that encountered in Earth's atmosphere. This result contradicts the widespread assumption that atmospheric water on Mars cannot exist in a supersaturated state, directly affecting our long-term representation of water transport, accumulation, escape, and chemistry on a global scale.

The atmosphere of Mars holds 10,000 times less water vapor than that of Earth. If precipitated at the surface, the martian atmospheric water would form a layer only 10 μm thick on average. However, water vapor on Mars is a very dynamic trace gas and is one of the most variable atmospheric constituents. The characterization of the seasonal and latitudinal variations of water vapor is based on 40 years of dedicated observations of its integrated column abundance (*1*–*5*), whereas water vapor vertical distribution has been only sparsely observed up to now. The latter is nevertheless a unique indicator of those vertical transport processes that control the hydrological activity of the planet (*6*). The first direct observations, obtained with the Auguste spectrometer on the Russian Phobos-2 spacecraft, revealed a sharp decline around 25 km (the hygropause level) connecting two layers of nearly constant concentration (*7*). The decline was interpreted to be the result of the conversion of water vapor into ice because a discrete cloud layer was observed in the altitude range of the vapor depletion zone. However, the Auguste data set covers a narrow equatorial strip and encompasses less than a martian month. Because of the lack of subsequent comparable measurements, our understanding of the vertical structure of water on Mars has been built on indirect observations (*8*–*10*) and theoretical studies of the martian climate by using general circulation models (GCMs). Near the surface, the vertical distribution is expected to be dominated by surface-atmosphere interactions (convection and frost sublimation and deposition), whereas at altitudes above 10 km the role of water ice clouds, which are nearly ubiquitous on Mars, should become dominant (*11*, *12*).

Martian climate models commonly assume that water vapor supersaturation cannot exist in the atmosphere: Any amount of water exceeding the equilibrium vapor pressure is immediately converted into ice (*11*). This hypothesis requires the existence of a condensation mechanism that acts instantaneously and ubiquitously. For this reason, the partial pressure of water vapor above the hygropause is expected to fall rapidly toward negligible values, establishing the perception of a martian water vapor profile resembling a two-step function, with water vapor well-mixed below the hygropause and sharply declining above. However, detailed microphysical models reveal that interactions between airborne particles and water vapor can affect the vertical confinement of water below the condensation level and its possible presence at higher altitudes (*13*). When condensation nuclei (assumed to be dust aerosols on Mars) are too rare, condensation is impeded and is thus unable to maintain water vapor at saturation level, leaving substantial amounts of excess vapor. Lack of condensation occurs frequently in the Earth's upper troposphere, where supersaturation levels as high as 50% with respect to ice have been reported (*14*).

The water vapor profile data set presented here was extracted from the SPICAM (Spectroscopy for the Investigation of the Characteristics of the Atmosphere of Mars) solar occultation observations. The SPICAM instrument onboard

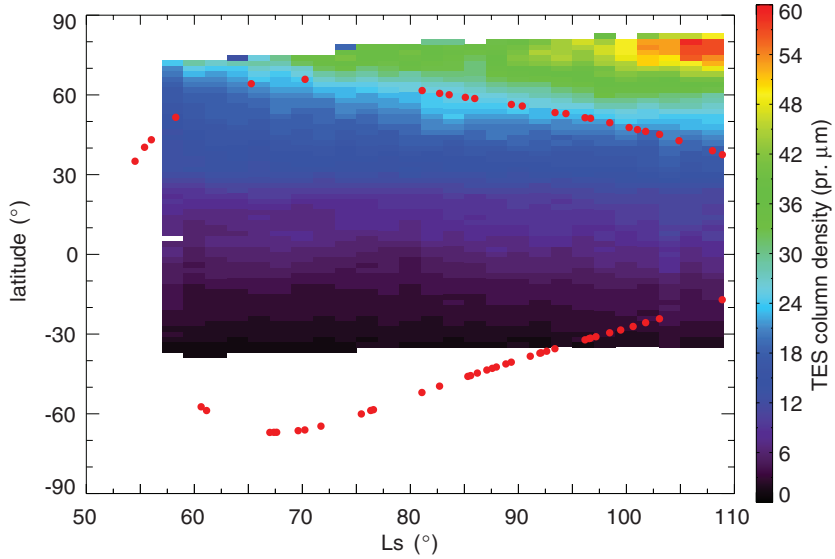

Fig. 1. SPICAM solar occultation positions shown by red dots as a function of L_s and latitude. TES water vapor column density retrievals (*19*) have been superimposed to indicate the corresponding activity of water vapor for the season during which the SPICAM measurements were taken.

[1]Laboratoire Atmosphères, Milieux, Observations Spatiales (LATMOS), 78280 Guyancourt, France. [2]Space Research Institute (IKI), 117997 Moscow, Russia. [3]Laboratoire de Météorologie Dynamique (LMD), 75252 Paris, France.

*To whom correspondence should be addressed. E-mail: luca.maltagliati@latmos.ipsl.fr